1

2

3

4

5

6

7

8

9

10

11

12

13

14

15

16

17

18

19

20

21

Methane oxidation over supported Pd catalysts prepared by magnetron sputtering

David Shaw, Justyna Kulczyk-Malecka, Peter J. Kelly, Aidan M. Doyle*

Faculty of Science and Engineering, Manchester Metropolitan University, Chester St., Manchester, M1 5GD, United Kingdom.

* Corresponding author: a.m.doyle@mmu.ac.uk

Abstract

While magnetron sputtering has been used to deposit metals onto a range of solid substrates, its application to produce porous heterogeneous catalysts in powder form is relatively unstudied. Here, magnetron sputtered Pd heterogeneous catalyst powders were prepared using a shaker operated at optimal experimental settings to give uniform coverage of the powders, and tested in the abatement of exhaust emissions in natural gas fuelled engines via the oxidation of methane. Pd nanoparticles were deposited onto alumina, titania and zeolite supports, in powder form. X-ray diffraction confirmed that the characteristic structure of each support was maintained following sputtering. The quantity of Pd increased (a) with deposition time and (b) as a function of support in the order alumina < zeolite < titania. The methane oxidation activity, measured as the temperatures at which 10% and 50% conversions were observed, T_{10} and T_{50}, increased with Pd content for each support and was most active over zeolite catalysts despite a greater amount of Pd present on titania. Overall, the findings demonstrate that magnetron sputtering is a viable method to prepare active precious metal based catalyst powders. Furthermore, this rapid one-step process is complete after 10-20 min deposition time and avoids any metal salt impurities or the need for solvent as required in traditional synthesis methods.

Keywords; Methane decomposition; dual-fuel; zeolite; exhaust emissions; magnetron sputtering.

1. Introduction

Natural gas contains up to ca. 95% methane and has received considerable attention in recent years as a fuel for heating and electricity generation. This is mainly due to the inexpensive and plentiful supply of methane/natural gas brought about by shale bed fracking, which is expected to continue for the foreseeable future [1]. It is also possible to produce methane renewably using biological processes that consume far less net carbon than fossil fuels (net carbon is not yet zero when associated energy requirements e.g. transportation, are taken into account). This 'biomethane' can be prepared in a number of ways e.g. from domestic waste in landfill sites or from the metabolic products of algal biomass [2].

Methane has the highest hydrogen to carbon ratio of any hydrocarbon, 4:1 versus ≤2:1 for diesel and, therefore, its use as a fuel generates less carbon dioxide than diesel. Dual-fuel technology allows methane to be used in a conventional compression ignition engine [3]. The engine operates by using two fuels simultaneously (when in dual–fuel mode), whereby combustion of the secondary fuel occurs alongside the compression-induced ignition of diesel [4,5]. The advantages of using methane as the secondary fuel are: lower operating costs, reduced carbon dioxide emissions and reduced levels of carbon based particulate matter. Taken together, these make dual-fuel a realistic possibility in the immediate term to decarbonise transport systems, particularly for heavy goods vehicles. The main barrier preventing the widespread adoption of dual-fuel powered engines is that the concentration of unburned methane in exhaust gases exceeds that allowed by current emissions legislation (developed for single fuel engines) [6,7]. As a result, there has been an intensive research effort to decompose methane in exhaust emissions [8,9]. The decomposition of methane by oxidation has been studied using reactions such as: steam reforming, partial oxidation, autothermal reforming, and dry reforming of methane (DRM) with carbon dioxide [10-14]. Complete methane oxidation occurs under stoichiometric or excess oxygen conditions and generates carbon dioxide and

72 water as products. Pd nanoparticles supported on high surface area metal oxide supports are
73 well-established catalysts for complete methane oxidation [15-20].
74 Precious metal heterogeneous catalysts are conventionally prepared by transferring metal(s)
75 from solutions of metal salts onto a support by e.g. ion-exchange or incipient wetness. The
76 solvent is then removed by heating and/or vacuum to leave behind the metal nanoparticles
77 dispersed on the support surface. While this method allows some flexibility to fine-tune the
78 properties of the final catalyst, e.g. metal nanoparticle size through variations in solution
79 chemistry and deposition method, there are associated disadvantages, such as the presence of
80 impurities and counter ions in the metal salts, and the need to remove the solvent by
81 evaporation, which consumes energy and may also cause undesirable changes to the catalyst.
82 Magnetron sputtering is a physical vapour deposition technique used to prepare thin films,
83 usually on planar surfaces or components. The process can be modified through the
84 introduction of a shaker to allow nanoparticles to be uniformly coated. Sputtering operates in
85 high vacuum whereby a plasma is created in a process gas, usually argon. Positive ions
86 generated in the plasma strike the metal target plate, or cathode, and remove target atoms by a
87 momentum exchange mechanism. The target atoms diffuse across the chamber and are
88 deposited on the solid substrate as a thin film. The magnetic field in the magnetron serves to
89 densify the plasma and improve the process efficiency. The preparation of catalysts by
90 magnetron sputtering offers a number of advantages over conventional methods including:
91 higher purity starting materials/catalysts, greater control of metal loadings and the absence of
92 a solvent, or any other ‘wet’ chemicals.
93 The majority of precious metal catalysts prepared using magnetron sputtering have focussed
94 on electrochemical systems containing Pt and Au deposited on metallic substrates [21]. Pd
95 film/nanoparticle deposition has been carried out on the following substrates: glass [22,23],
96 glucose [24] silicon wafer [25,26], stainless steel [27], and a number of forms of carbon; glassy

carbon [28], carbon black [29], carbon paper [30], carbon cloth [31], carbon nanotubes [32] and highly ordered pyrolytic graphite (HOPG) [33]. There are relatively few accounts of Pd nanoparticles deposited on commercial catalyst supports in powder form. Pd sputtered onto alumina [34] and carbon black [35] were active heterogeneous catalysts in hydrogenation reactions, and ammonia borane was found to decompose over Pd sputtered mesoporous silica MCM-48 [36].

To our knowledge, there are no reports of methane oxidation over Pd based powder catalysts prepared using magnetron sputtering. Here, we prepare Pd on alumina, titania and zeolite supports using magnetron sputtering, and test their catalytic activity in complete methane oxidation. The results show that both the quantity of Pd deposited and the catalytic activity are dependent on the choice of underlying support.

2. Experimental

2.1 Pd deposition by magnetron sputtering

The following is a list of the suppliers and reagents: activated alumina, Sigma Aldrich; titania, PC 500, Millennium Inorganic Chemicals; Y-zeolite Si/Al 30, Zeolyst International; Pd target PiKem 99.99%. 5.0 g of catalyst support (alumina, titania or zeolite) was placed onto a SignalForce™ Data Physics shaker inside an in-house built magnetron sputtering vacuum chamber, Fig. 1, in which a single 75 mm diameter unbalanced magnetron was installed in the chamber roof in the 'sputter down' configuration. The shaker, positioned directly underneath the magnetron at a separation of 8 cm, was adjusted in terms of oscillation frequency and amplitude to optimise the movement of the powder supports within a 10 cm diameter dish attached to the shaker. The chamber was sealed and the pressure was reduced to a base pressure of $< 4.0 \times 10^{-3}$ Pa using a Leybold 250 turbo pump and Edwards 28 rotary pump. Once the desired base pressure was reached, the chamber was backfilled with argon at a flow rate of 10

ml min^{-1} to maintain an operating pressure of 0.5 Pa. The target was sputtering in pulsed DC mode at 100 W and 100 kHz pulse frequency (60% duty) using an Advanced Energy DC Pinnacle Plus™ power supply. The Data Physics shaker was then switched on and separate batches of support materials were sputtered coated with Pd for durations of 10, 15 and 20 min. Following deposition, the system was allowed to cool for 15 min before venting and removal of the coated powder.

2.2 Characterisation

X-ray diffraction (XRD) was conducted in ambient conditions using a Panalytical X'Pert Powder diffractometer with Cu Kα radiation (λ = 1.5406 Å). All powder diffraction patterns were recorded from 4 to 120 ° 2θ with step size 0.013 ° and step time 50 s, using an X-ray tube operated at 40 kV and 30 mA with fixed ¼ ° anti-scatter slit. A Rigaku NEX-CG X-ray fluorescence (XRF) spectrometer was used for elemental analysis using the loose powder method under vacuum. Nitrogen adsorption/desorption measurements were carried out using a Micromeritics ASAP 2020 surface area analyser at -196 °C. Samples were degassed under vacuum ($p < 10^{-3}$ Pa) for 12 h at 300 °C prior to analysis. BET surface areas of the samples were calculated in the relative pressure range 0.05-0.30.

2.3 Catalytic tests

The catalytic activity of each sample was studied in a quartz fixed bed reactor, Fig. 2, placed inside a temperature controlled furnace (Carbolite type 3216, Tempatron, PID500/110/330). 0.2 g of catalyst was calcined in air for 4 h at 550 °C and placed in a quartz tube (10 mm diameter, 1 mm thickness) between quartz wool plugs. A feed mixture of 50 ml min^{-1} comprising CH_4:O_2:He in ratios 5:10:35 ml min^{-1}, which is equivalent to 10%, 20% and 70%, respectively, was used in all catalytic tests. Methane (c.99.9995%) and oxygen (c.99.999%)

147 gases were supplied from lecture bottles (CKGAS filled to 200 Bar at 15 °C) and regulated
148 using single stage CONCOA 302 series gas regulators. The flow of each gas was maintained
149 using Bronkhorst UK model F-201CV mass flow controllers. The reaction products were
150 monitored by a Hewlett Packard 5890 series II gas chromatograph equipped with a Carboxen
151 1010 plot fused silica capillary column (30 m x 0.53 mm) connected *via* a 6-way gas sampling
152 valve to a thermal conductivity detector. Measurements were recorded at 25 °C intervals (after
153 holding at that temperature for 5 min) using a heating rate of 10 °C min^{-1}.
154
155 **3. Results & discussion**
156 **3.1 Characterisation**
157 XRD diffraction patterns, Fig. 3, confirm the presence of Pd and that the characteristic structure
158 for each catalyst support remains intact after exposure to the plasma. Table 1 shows that the
159 amount of Pd deposited, determined by XRF, increases with deposition time, as is expected for
160 this process. Furthermore, the Pd is deposited at a regular rate, evidenced by the proportional
161 increase in mass as a function of time e.g. on titania, 3.62 wt% was deposited after 10 min and
162 7.36 wt% after 20 min, an approximate doubling of Pd with run time. However, the amounts
163 of Pd deposited varied considerably between the supports, increasing in the order alumina <
164 zeolite < titania. When these differences are quantified by calculating the average wt%
165 deposited on a given support over the three exposure times relative to that of titania (100%),
166 the relative amounts of Pd deposited was 48% on zeolite and 19% on alumina.
167 It is difficult to assign with certainty the underlying reasons for these differences. However,
168 there are examples in the literature that suggest adhesion issues when depositing Pd on alumina,
169 whereas the authors have successfully used the technique here to deposit Pt-group metals onto
170 titania particles, including PC500 [37]. It has been speculated that this might be related to the
171 surface sticking coefficient or the dielectric constant of the support. In the latter case, the more

insulating nature of alumina may result in the particles becoming electrically charged whilst in the magnetron plasma and repelling the incident argon ion bombardment which occurs during sputtering and strongly influences film growth and adhesion [38]. Table 1 shows the surface areas of the Pd deposited samples increase in the order titania 80-117 $m^2 g^{-1}$, alumina 112-143 $m^2 g^{-1}$ and zeolite 730-743 $m^2 g^{-1}$. All surface areas are consistent with those expected for these underling supports. We are unable to provide conclusive reasons for changes in surface area e.g. 117 $m^2 g^{-1}$ for the 15 min deposited sample on titania versus 80 $m^2 g^{-1}$ for 10 min. In any case, there are too few samples overall from which to draw definitive trends in surface areas for the study presented here.

3.2 Catalyst testing

The complete oxidation of methane is used both as a test reaction for the Pd sputtered catalysts and to determine their suitability in engine exhaust emissions treatment. Carbon monoxide was not detected in any of the experiments. All substrates containing Pd were catalytically active and the results are shown as light-off curves in Fig. 4. The data for 10 min Pd deposition, Fig. 4(a), clearly show that the catalytic activities (measured from conversion temperatures) increased in the order: alumina < titania < zeolite. Longer deposition times of 15 min, Fig. 4(b), and 20 min, Fig. 4(c), caused increases in activity overall by shifting methane conversion to lower temperatures. It is interesting to note that the titania supported catalysts were more active than the zeolite catalysts at lower reaction temperatures for 15 and 20 min deposition times. This enhanced methane oxidation activity was observed at temperatures up to 320 °C for 15 min deposition, and up to 275 °C for 20 min. The superior activity of titania at low reaction temperatures also occurred, albeit to a much lower degree, for 10 min deposition as evidenced by the detection of trace quantities of the reaction product CO_2 by GC (not shown) for titania at 200 °C, which was not detected for zeolite at the same temperature. Methane conversions

became approximately equal (<2%) for titania and zeolite at 250 °C. The authors acknowledge that the minor differences in conversions at the lower temperature ranges may be explained by experimental error, so their relevance to the overall conclusions should be considered tentatively. Kinetic data calculated up to 30% conversion gave activation energies in the range 106-116 kJ mol^{-1} for alumina, 76.5-83.8 kJ mol^{-1} for titania and 89.9-111 kJ mol^{-1} for zeolite, Table 1.

These results may be considered further by exploring the temperatures required for 10% and 50% conversion, T_{10} and T_{50}, as a function of Pd content, Fig. 5. The trends here reinforce the findings that catalytic activities increase with deposition time, manifested by a general decrease in both T_{10} and T_{50}. For example, increasing the deposition time from 10 to 20 min caused a decrease in T_{50} values from 413 °C to 378 °C for alumina, 346 °C to 305 °C for titania and 320 °C to 285 °C for zeolite. Escandón et al. compared methane oxidation over various supports and recorded a T_{50} value of 334 °C on alumina (0.84 wt% Pd) versus 483 °C on titania (0.90 wt% Pd) [39]. While alumina is a well-established and active support for a range of heterogeneously catalysed reactions it appears that it is relatively unsuited to applications involving magnetron sputtering, at least using the procedure described here.

The relative activities at lower reaction temperatures are more accurately captured in the T_{10} readings. The zeolite catalyst is the most active after 10 min deposition, T_{10} is 283 °C, versus 300 °C for titania, while titania is more active for 15 min, 271 °C, and 20 min, 242 °C, relative to the zeolite; 284 °C and 257 °C, respectively. These trends are in agreement with the profiles seen in the light-off curves, Fig. 4. We recently reported a methane oxidation T_{50} value of 288 °C for a Pd-zeolite prepared by conventional ion-exchange and ultrasonic treatment, using the same catalyst testing rig and conditions as in this paper [19]. The fact that this T_{50} value is almost identical to the zeolite catalyst prepared using 20 min sputtering, 285 °C validates the application of magnetron sputtering to the preparation of catalyst powders via relatively rapid

production times (20 min) and without the need for ultrasonic treatment or solvent removal. Furthermore, this magnetron sputtered catalyst contained less Pd, 3.04 wt%, Table 1, versus 5.25 wt% on the ion-exchanged sample.

The enhanced reactivity of the zeolite supported Pd catalysts can be explained primarily by the presence of more numerous and much stronger acid sites than those on alumina and titania supports. Density functional theory (DFT) calculations confirmed that a bond interaction exists between the acidic H^+ of zeolite and the O atom of PdO, and that such acid sites are necessary for methane activation and sintering prevention [40,41]. Dai et al. showed that Lewis acid sites are required to prepare highly dispersed Pd/ZSM-5 catalysts [42]. In a separate study comparing zeolites in H^+ and Na^+ from, the interaction between zeolite acid sites and PdO nanoparticles was shown to reduce PdO sintering such that better stability was observed for the more acidic H^+ support [43]. Friberg et al. explored the effects of Si/Al ratio of zeolites on methane oxidation and showed that zeolite acid sites increased the dispersion of Pd nanoparticles and even allowed the formation of monoatomic Pd^{2+} species [44]. The Si/Al ratios of zeolite in that study ranged from 40-969 so, for comparison purposes, the zeolite used in our paper, Si/Al = 30, can be considered 'low'; this value is consistent with a 'high' number of acid sites, which could explain greater catalytic activity on the zeolite supports. For the results presented in our paper, the superior activity over zeolite supported catalysts is, therefore, explained by negatively charged sites in the zeolite framework (countered by e.g. H^+) that provide anchoring locations to which positively charged species in the plasma attach. The higher bond energies of these interactions make the zeolite surface more attractive to the Pd species both in the plasma and on the surface, which compensates for the additional surface energy associated with the formation of smaller nanoparticles.

Further evidence to support this can be seen by considering the reaction rates in Table 1, where the rate *per unit mass of Pd* typically decreases with increasing Pd coverage. These decreases

247 can be partially explained by the lower temperatures needed to accurately display the results
248 i.e. 350 °C for 10 min, 320 °C for 15 min and 300 °C for 20 min. However, the extent to which
249 these reaction rates decrease differs greatly for the supports. Comparing Pd deposition for 10
250 and 20 min, the rate drops 87% from 12.7 to 1.59 mmoles CH_4/min g Pd on alumina, 61% from
251 16.7 to 6.56 mmoles CH_4/min g Pd on titania, but drops only 34% from 51.8 to 34.1 mmoles
252 CH_4/min g Pd on zeolite. These differences are attributed to the combination of the (a) stronger
253 interaction of Pd/PdO to the acid sites in zeolite and (b) confinement within zeolite cages,
254 which together restrict the growth of Pd particles relative to the alumina and titania supports
255 giving more highly dispersed Pd/PdO on the zeolite catalysts [45,46]. The authors do not have
256 HR-TEM facilities to accurately image the Pd/PdO nanoparticles so we fully acknowledge that
257 our explanation is tentatively based on the combination/comparison of the results presented
258 here with published works.
259 Other factors that may contribute to the zeolite activity are their higher surface areas or that the
260 zeolite acid site-PdO interaction makes the zeolite more hydrophobic by decreasing the
261 adsorption binding strength of water (present as a combustion product) which would otherwise
262 poison the active surface and increase Pd sintering during reaction [47]. Zeolites may also
263 increase activity in oxidation reactions by increasing the reducibility of PdO relative to non-
264 acidic supports [48].
265
266 **4. Conclusions**
267 Magnetron sputtering is a feasible method to rapidly prepare catalyst powders on commercially
268 relevant supports that are active in complete methane oxidation. The quantity of Pd deposited
269 varied between supports and was found to be highest on titania and lowest on alumina. Zeolite
270 Y was the most catalytically active support even when using a lower mass ratio of Pd than that
271 on titania. Considering the number of reactions where zeolites are used and the benefits of

magnetron sputtering over conventional catalyst preparation methods, magnetron sputtering is well placed to be applied in future to prepare highly active catalytic materials containing other precious and/or non-precious metals.

Acknowledgments

Funding: This work was funded by G-volution ltd.

References

[1] U. Izquierdo, V.L. Barrio, J. Requies, J.F. Cambra, M.B. Güemez, P.L. Arias, Tri-reforming: A new biogas process for synthesis gas and hydrogen production, Int. J. Hydrog. Energy 38 (2013) 7623-7631. https://doi.org/10.1016/j.ijhydene.2012.09.107

[2] X. Shan, Y. Qian, L. Zhu, X. Lu, Effects of EGR rate and hydrogen/carbon monoxide ratio on combustion and emission characteristics of biogas/diesel dual fuel combustion engine, Fuel 181 (2016) 1050-1057. https://doi.org/10.1016/j.fuel.2016.04.132

[3] C. Abagnale, M.C. Cameretti, L. De Simio, M. Gambino, S. Iannaccone, R. Tuccillo, Numerical simulation and experimental test of dual fuel operated diesel engines, Appl. Therm. Eng. 65 (2014) 403-417. http://dx.doi.org/10.1016/j.applthermaleng.2014.01.040

[4] J. Benajes, A. García, J. Monsalve-Serrano, I. Balloul, G. Pradel, An assessment of the dual-mode reactivity controlled compression ignition/conventional diesel combustion capabilities in a EURO VI medium-duty diesel engine fueled with an intermediate ethanol-gasoline blend and biodiesel, Energy Convers. Manage. 123 (2016) 381-391. https://doi.org/10.1016/j.enconman.2016.06.059

[5] J. Klimstra, 11 - Fuel flexibility with dual-fuel engines A2 - Oakey, John, in: Fuel Flexible Energy Generation, Woodhead Publishing, Boston, 2016, pp. 293-304.

[6] B. Bharathiraja, T. Sudharsanaa, A. Bharghavi, J. Jayamuthunagai, R. Praveenkumar, Biohydrogen and Biogas – An overview on feedstocks and enhancement process, Fuel 185 (2016) 810-828. https://doi.org/10.1016/j.fuel.2016.08.030

[7] M. Crippa, G. Janssens-Maenhout, D. Guizzardi, S. Galmarini, EU effect: Exporting emission standards for vehicles through the global market economy, J. Environ. Manage. 183, Part 3 (2016) 959-971. https://doi.org/10.1016/j.jenvman.2016.09.068

[8] Y. Karagöz, T. Sandalcı, U.O. Koylu, A.S. Dalkılıç, S. Wongwises, Effect of the use of natural gas–diesel fuel mixture on performance, emissions, and combustion characteristics of a compression ignition engine, Adv. Mech. Eng. 8 (2016) 1-13. https://doi.org/10.1177/1687814016643228

[9] B. Challen, R. Baranescu, Diesel Engine Reference Book. Society of Automotive Engineers, 1999.

[10] R. Horn, R. Schlögl, Methane activation by heterogeneous catalysis, Catal. Lett. 145 (2015) 23-39. https://doi.org/10.1007/s10562-014-1417-z

[11] B.C. Enger, R. Lødeng, A. Holmen, A review of catalytic partial oxidation of methane to synthesis gas with emphasis on reaction mechanisms over transition metal catalysts, Appl. Catal. A: Gen. 346 (2008) 1-27. https://doi.org/10.1016/j.apcata.2008.05.018

[12] P. Gélin, M. Primet, Complete oxidation of methane at low temperature over noble metal based catalysts: a review, Appl. Catal. B: Environ. 39 (2002) 1-37. https://doi.org/10.1016/S0926-3373(02)00076-0

[13] J.H. Lunsford, Catalytic conversion of methane to more useful chemicals and fuels: a challenge for the 21st century, Catal. Today 63 (2000) 165-174. https://doi.org/10.1016/S0920-5861(00)00456-9

[14] J. Kamieniak, P.J. Kelly, C.E. Banks, A.M. Doyle, Methane emission management in a dual-fuel engine exhaust using Pd and Ni hydroxyapatite catalysts, Fuel 208 (2017) 314-320. https://doi.org/10.1016/j.fuel.2017.07.012

[15] A.W. Petrov, D. Ferri, F. Krumeich, M. Nachtegaal, J.A. van Bokhoven, O. Kröcher, Stable complete methane oxidation over palladium based zeolite catalysts, Nat. Commun. 9:2545 (2018). https://doi.org/10.1038/s41467-018-04748-x

[16] R. Gholami, M. Alyani, K.J. Smith, Deactivation of Pd catalysts by water during low temperature methane oxidation relevant to natural gas vehicle converters, Catalysts 5 (2015) 561–594. https://doi.org/10.3390/catal5020561

[17] Y. Li, J.N. Armor, Catalytic combustion of methane over palladium exchanged zeolites, Appl. Catal. B: Environ. 3 (1994) 275–282. https://doi.org/10.1016/0926-3373(94)0006Z-H

[18] C. Montes de Correa, A.L. Villa, Combustion of methane over palladium ZSM-5 and mordenite catalysts, Appl. Catal. B: Environ. 10 (1996) 313–323. https://doi.org/10.1016/S0926-3373(96)00039-2

[19] A.M. Doyle, R. Postolache, D. Shaw, R. Rothon, L. Tosheva, Methane oxidation over zeolite catalysts prepared from geothermal fluids, Microporous and Mesoporous Mater. 285 (2019) 56-60. https://doi.org/10.1016/j.micromeso.2019.04.069

[20] S. Hajimirzaee, A.M. Doyle, 3D printed catalytic converters with enhanced activity for low-temperature methane oxidation in dual-fuel engines, Fuel 274 (2020) 117848. https://doi.org/10.1016/j.fuel.2020.117848

[21] O.K. Alexeeva, V.N. Fateev, Application of the magnetron sputtering for nanostructured electrocatalysts synthesis, Int. J. Hydrog. Energy 41 (2016) 3373-3386 https://doi.org/10.1016/j.ijhydene.2015.12.147

[22] D. Horwat, D.I. Zakharov, J.L. Endrino, F. Soldera, A. Anders, S. Migot, R. Karoum, Ph. Vernoux, J.F. Pierson, Chemistry, phase formation, and catalytic activity of thin palladium-containing oxide films synthesized by plasma-assisted physical vapor deposition, Surf. Coat. Tech. 205 (2011) S171-S177. https://doi.org/10.1016/j.surfcoat.2010.12.021

[23] E. Slavcheva, G. Ganske, U. Schnakenberg, Sputtered Pd as hydrogen storage for a chip-integrated microenergy system, Sci. World J. (2014) Article ID 146126 http://dx.doi.org/10.1155/2014/146126

[24] H.-Y. Park, I. Jang, N. Jung, Y.-H. Chung, J. Ryu, I.Y. Cha, H.-J. Kim, J. H. Jang, S.J. Yoo, Green synthesis of carbon-supported nanoparticle catalysts by physical vapor deposition on soluble powder substrates, Sci. Rep. 5 (2015) 14245 https://doi.org/10.1038/srep14245

[25] R.K Joshi, S. Krishnan, M. Yoshimura, A. Kumar, Pd nanoparticles and thin films for room temperature hydrogen sensor, Nanoscale Res. Lett. 4(10) (2009) 1191–1196. https://doi.org/10.1007/s11671-009-9379-6

373 [26] A.L Thomann, C. Charlesd, P. Brault, C. Laure, R. Boswelld, Plasma Sources Sci.
374 Technol. 7 (1998) 245–251.

375 [27] Y. Huang, R. Dittmeyer. Preparation of thin palladium membranes on a porous support
376 with rough surface, J. Membrane Sci. 302 (2007) 160-170.
377 https://doi.org/10.1016/j.memsci.2007.06.040

378 [28] V. Singh C. Cassidy F. Abild-Pedersen J.-H. Kim, K. Aranishi, S. Kumar, C. Lal, C.
379 Gspan, W. Grogger, M. Sowwan, Engineering high-performance Pd core–MgO porous shell
380 nanocatalysts via heterogeneous gas-phase synthesis, Nanoscale 7 (2015) 13387.
381 https://doi.org/10.1039/c5nr02663f

382 [29] G.M. Veith, A.R. Lupini, L. Baggetto, J.F. Browning, J.K. Keum, A. Villa, L. Prati, A. B.
383 Papandrew, G.A. Goenaga, D.R. Mullins, S.E. Bullock, N.J. Dudney, Evidence for the
384 formation of nitrogen-rich platinum and palladium nitride nanoparticles, Chem. Mater. 25
385 (2013) 4936-4945. https://doi.org/10.1021/cm403224m

386 [30] F. Sarto, E. Castagna, M. De Francesco, T.M. Dikonimos, L. Giorgi, S. Lecci, M.
387 Sansovini, V. Violante, Morphology and electrochemical properties of Pd-based catalysts
388 deposited by different thin-film techniques, Int. J. Hydrog. Energy 39 (2014) 14701-14711.
389 https://doi.org/10.1016/j.ijhydene.2014.07.038

390 [31] I. Bieloshapka, P. Jiricek, M. Vorokhta, E. Tomsik, A. Rednyk, R. Perekrestov, K. Jurek,
391 E. Ukraintsev, K. Hruska, O. Romanyuk, B. Lesiakc, Pd-catalysts for DFAFC prepared by
392 magnetron sputtering, Appl. Surf. Sci. 419 (2017) 838–846.
393 https://doi.org/10.1016/j.apsusc.2017.05.035

394 [32] K. Jukk, N. Alexeyeva, P. Ritslaid, J. Kozlova, V. Sammelselg, K. Tammeveski,
395 Electrochemical reduction of oxygen on heat-treated Pd nanoparticle/multi-walled carbon
396 nanotube composites in alkaline solution, Electrocatalysis 4 (2013) 42-48.
397 https://doi.org/10.1007/s12678-012-0117-y

398 [33] L. Arroyo-Ramírez, D. Rodríguez, W. Otaño, C.R. Cabrera, Palladium nanoshell catalysts
399 synthesis on highly ordered pyrolytic graphite for oxygen reduction reaction, ACS Appl. Mater.
400 Interfaces 4 (2012) 2018-2024. https://doi.org/10.1021/am201860r

401 [34] P.R. Ellis, C.M. Brown, P.T. Bishop, J. Yin, K. Cooke, W.D. Terry, J. Liu, F. Yin, R.E.
402 Palmer, The cluster beam route to model catalysts and beyond, Faraday Discuss. 188 (2016)
403 39. https://doi.org/10.1039/c5fd00178a

404 [35] M. Ali, G. Abarca, D. Eberhardt, A. Gual, F. Bernardi, S.R. Teixeira, J. Dupont, "Save
405 money" during hydrogenation reactions by exploiting the superior performance of Pd-NPs
406 deposited on carbon black by magnetron sputtering, Tetrahedron 73 (2017) 5593-5598.
407 https://doi.org/10.1016/j.tet.2016.11.043

408 [36] G. Xin, J. Yang, W. Li J. Zheng, X. Li, Catalytic Thermal decomposition of ammonia–
409 borane by well-dispersed metal nanoparticles on mesoporous substrates prepared by magnetron
410 sputtering, Eur. J. Chem. 34 (2012) 5722-5728. https://doi.org/10.1002/ejic.201200752

411 [37] M. Bernareggi, G.L. Chiarello, G. West, M. Ratova, A.M. Ferretti, P.J. Kelly, E. Selli, Cu
412 and Pt clusters deposition on TiO_2 powders by DC magnetron sputtering for photocatalytic

hydrogen production, Catal. Today 326 (2019) 15-21. https://doi.org/10.1016/j.cattod.2018.07.011

[38] V. Jayaraman, Y.S. Lin, M. Pakala, R.Y. Lin, Fabrication of ultrathin metallic membranes on ceramic supports by sputter deposition, J. Membrane Science 99 (1995) 89-100. https://doi.org/10.1016/0376-7388(94)00212-H

[39] L.S. Escandón, S. Ordóñez, A. Vega, F.V. Díez, Oxidation of methane over palladium catalysts: effect of the support, Chemosphere 58 (2005) 9-17. https://doi.org/10.1016/j.chemosphere.2004.09.012

[40] J.-g. Wang, C.-j. Liu, Density functional theory study of methane activation over PdO/HZSM-5, J. Mol. Catal. A Chem. 247 (2006) 199-205. https://doi.org/10.1016/j.molcata.2005.11.054

[41] J.-g. Wang, C.-j. Liu, Z. Fang, Y. Liu, Z. Han, DFT Study of Structural and Electronic Properties of PdO/HZSM-5, J. Phys. Chem. B 108 (2004) 1653-1659. https://doi.org/10.1021/jp035779o

[42] Q. Dai, Q. Zhu, Y. Lou, X. Wan, Role of Brønsted acid site during catalytic combustion of methane over PdO/ZSM-5: Dominant or negligible? J. Catal. 57 (2018) 29–40. https://doi.org/10.1016/j.jcat.2017.09.022

[43] K. Okumura, S. Matsumoto, N. Nishiaki, M. Niwa, Support effect of zeolite on the methane combustion activity of palladium, Appl. Catal. B: Environ. 40 (2003) 151-159. https://doi.org/10.1016/S0926-3373(02)00149-2

[44] I. Friberg, N. Sadokhina, L. Olsson, The effect of Si/Al ratio of zeolite supported Pd for complete CH_4 oxidation in the presence of water vapor and SO_2, Appl. Catal. B: Environ. 250 (2019) 117-131. https://doi.org/10.1016/j.apcatb.2019.03.005

[45] N. Wang, Q. Sun, R. Bai, X. Li, G. Guo, J. Yu, In situ confinement of ultrasmall Pd clusters within nanosized Silicalite-1 zeolite for highly efficient catalysis of hydrogen generation. J. Am. Chem. Soc. 138 (2016) 7484– 7487. https://doi.org/10.1021/jacs.6b03518

[46] A.W. Petrov, D. Ferri, F. Krumeich, M. Nachtegaal, J.A. van Bokhoven, O. Kröcher, Stable complete methane oxidation over palladium based zeolite catalysts. Nat. Commun. 9 (2018) 2545 https://doi.org/10.1038/s41467-018-04748-x

[47] P. Losch, W. Huang, O. Vozniuk, E.D. Goodman, W. Schmidt, M. Cargnello, Modular Pd/zeolite composites demonstrating the key role of support hydrophobic/hydrophilic character in methane catalytic combustion. ACS Catal. 9 (2019) 4742−4753. https://doi.org/10.1021/acscatal.9b00596

[48] Y. Li, J.N. Armor, Catalytic combustion of methane over palladium exchanged zeolites. Appl. Catal. B: Environ. 3 (1994) 275– 282, https://doi.org/10.1016/0926-3373(94)0006Z-H

Table 1: Pd wt% as determined by XRF, BET surface area (S_{BET}), thermodynamic data and reaction rate for methane oxidation.

Support	Sputter time (min)	Pd loading (wt%)	S_{BET} ($m^2\ g^{-1}$)	E_A (kJ mol^{-1})	Rate (mmoles CH_4/min g Pd)[a]
Alumina	10	0.58	146	106	12.7
	15	1.04	112	116	2.13
	20	1.48	143	114	1.59
Titania	10	3.62	80	81.3	16.7
	15	4.78	117	76.5	19.4
	20	7.36	80	83.8	6.56
Y zeolite	10	1.66	730	111	51.8
	15	2.74	743	89.9	39.9
	20	3.04	735	93.5	34.1

[a] Reaction rates are expressed at different temperatures to ensure that CH_4 conversion % were inside the range 0-100% for all three supports: 350 °C for 10 min, 320 °C for 15 min and 300 °C for 20 min.

List of figure captions:

Fig. 1: Schematic diagram of magnetron sputtering set up.

Fig. 2: PFD of catalyst testing rig; the zig-zag pattern added to the line between v6 and the GC TCD/FID represents heating tape.

Fig. 3: XRD powder patterns of alumina, titania and zeolite supports following sputtering; Pd peaks are indicated with an *.

Fig. 4: Data for CH_4 conversion vs. reaction temperature in a fixed bed reactor over alumina, titania and zeolite catalyst supports for Pd sputter times of (a) 10 min, (b) 15 min and (c) 20 min. Total flow rate of feed mixture is 50 ml min^{-1} comprising CH_4:O_2:He = 10%:20%:70%.

Fig. 5: T_{10} (lower) and T_{50} (higher) values for CH_4 conversion vs Pd content. Total flow rate of feed mixture is 50 ml min^{-1} comprising CH_4:O_2:He = 10%:20%:70%.

Figures:

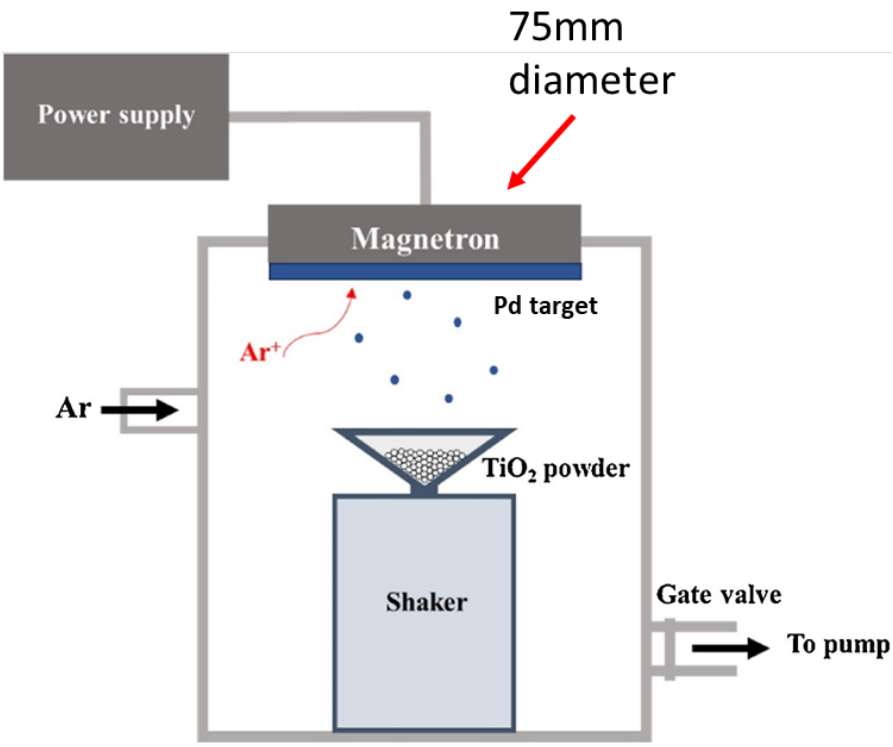

Fig. 1.

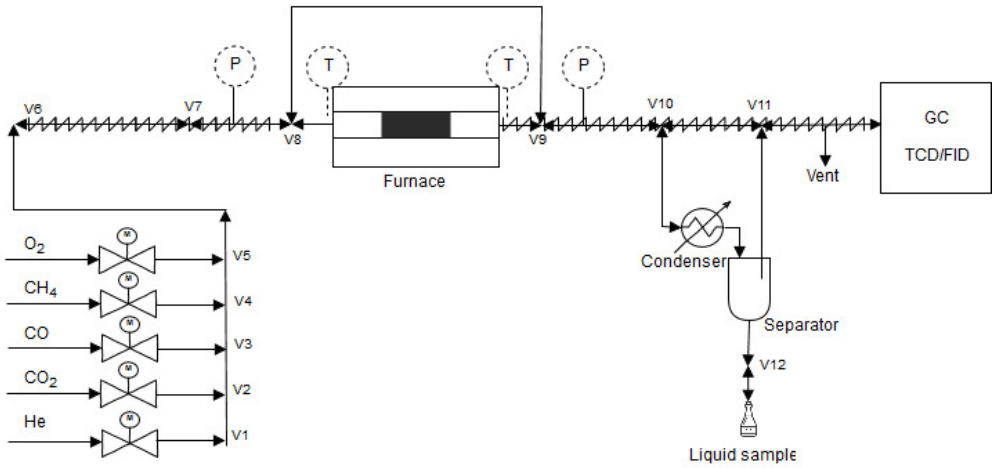
P
T
T
P
V6
V7
V8
V9
V10
V11
Furnace
GC
TCD/FID
Vent
Condenser
Separator
V12
Liquid sample
O_2
CH_4
CO
CO_2
He
V5
V4
V3
V2
V1

Fig. 2.

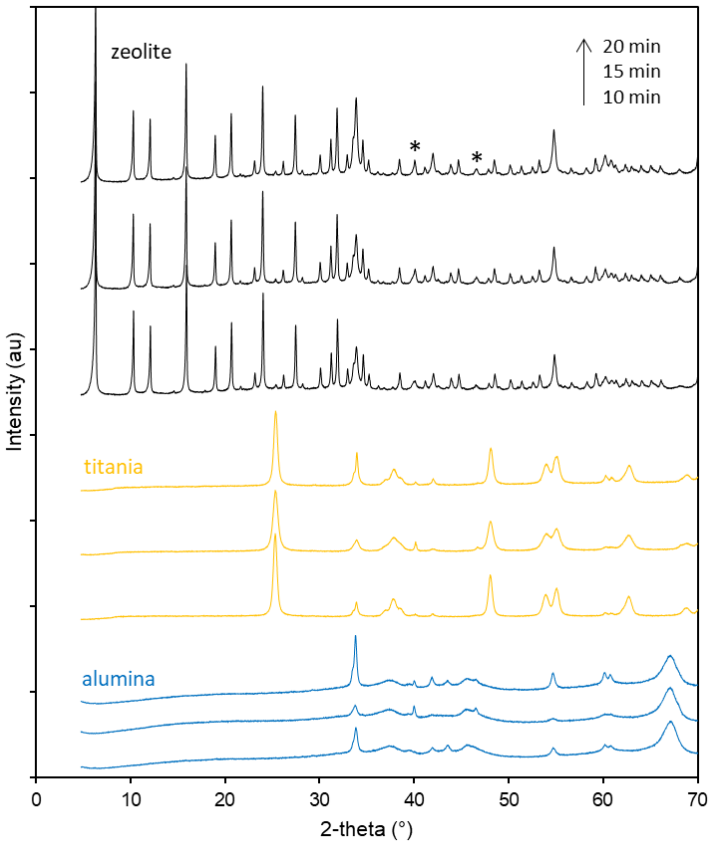
zeolite
20 min
15 min
10 min
*
*
titania
alumina
Intensity (au)
0
10
20
30
40
50
60
70
2-theta (°)

Fig. 3.

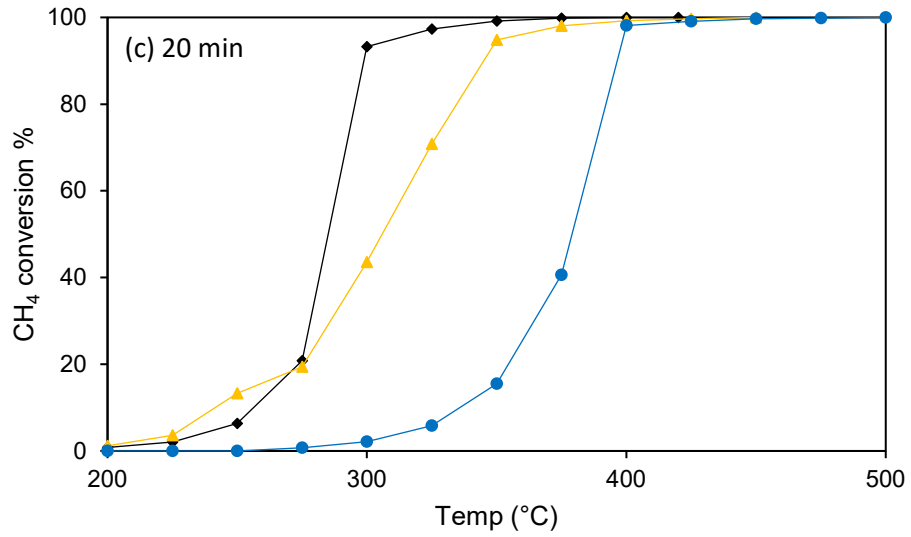

541

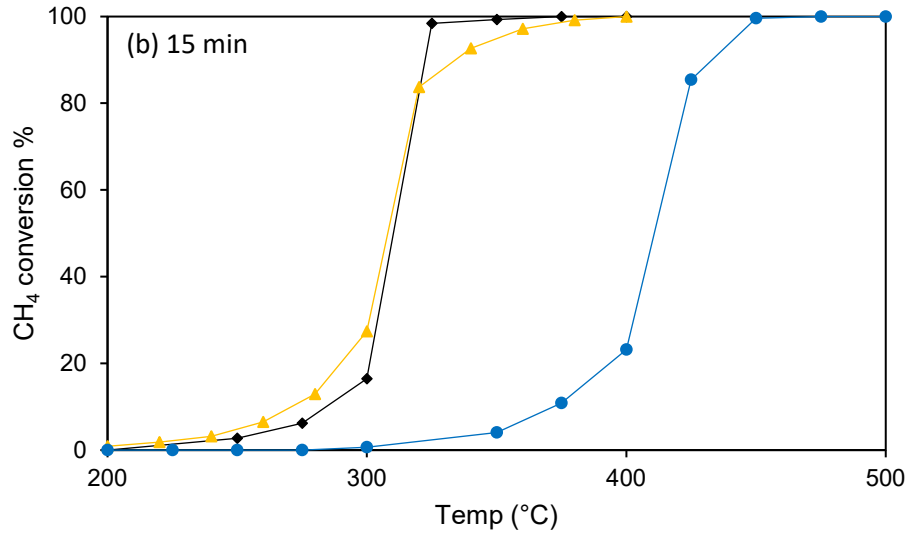

542

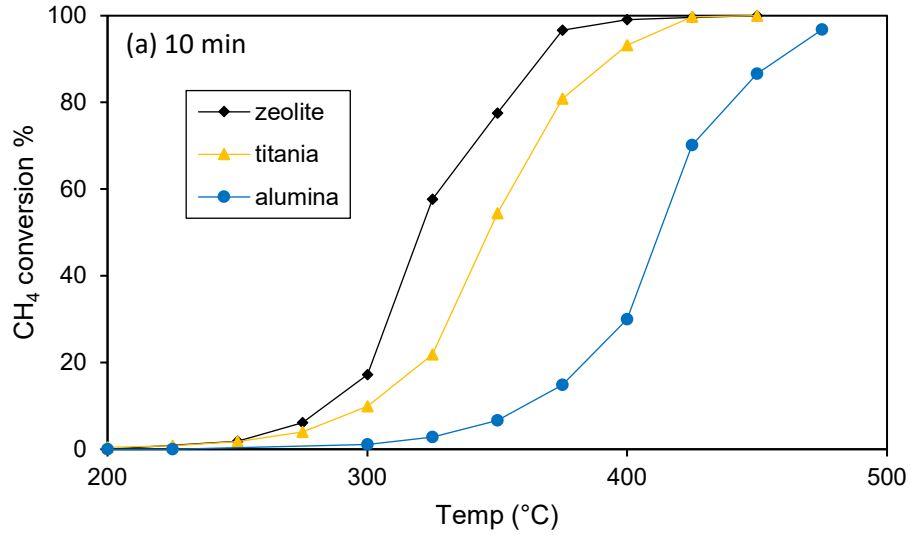

543

544 Fig. 4.

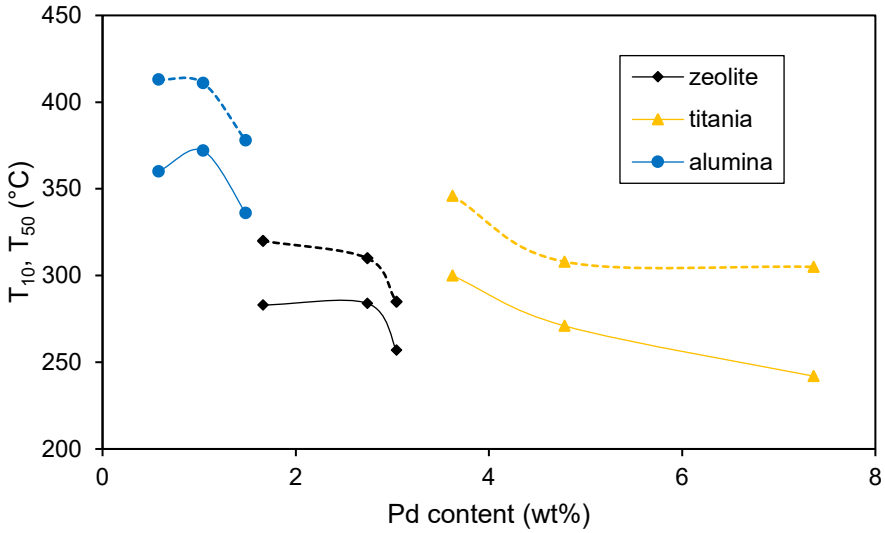

545

546 Fig. 5.

547